

Polarized Diversity Compact Planar MIMO Antenna for Wireless Access Point Applications

Alireza Moradi¹, *, Razali Ngah¹, and Mohsen Khalily²

Abstract—In this paper, a wideband polarization diversity multi-input multioutput (MIMO) antenna system is proposed. The structure of the proposed antenna consists of four wideband coplanar waveguide (CPW)-fed monopole antennas with a common ground plane and radiated element. The simulated and measured -10 dB impedance bandwidth is 20% (2.25–2.75 GHz), which covers WiFi (2.4 GHz) and LTE (2.6 GHz) frequency bands. The MIMO antenna system is applied to both an indoor and outdoor wireless access point (WAP) at the covered frequency bands. Due to the common structure of elements in the proposed MIMO antenna, an acceptable mutual coupling between the antennas ports is critical. Hence, a new parasitic element structure is presented to improve mutual coupling between the antenna ports. Acceptable values for the coupling coefficient (< -14 dB) are achieved by adding the parasitic element. The presented antenna system provides a nearly omnidirectional radiation pattern with an orthogonal mode of linear polarization. The results show a polarization diversity gain of 10 dB and an envelope correlation coefficient of less than 0.2. Moreover, each antenna port possesses peak gains of 5.33–6.97 dBi and efficiencies of 51.5–57%. A comparison between the simulation results and experimental measurements reveals good agreement between the two, confirming the validity of the proposed design.

1. INTRODUCTION

Currently, multiple-input multiple-output (MIMO) technology is a very important structure in wireless communication systems, such as wireless local area network (WLAN), long term evolution (LTE), and fifth generation (5G) systems [1]. High-speed data transfer rate and large channel capacity are among the most advantageous features of MIMO technology in wireless communication systems. Many researchers have focused on multiband and wideband MIMO antenna systems due to the demand for these types of antennas. Coplanar waveguide (CPW) line feed is a method that has been adopted for the design of MIMO antennas, due to its numerous remarkable features, including wide bandwidth, easy integration with MMICs and active devices, and simple uniplanar structure [2–4]. In recent years, several multiband and wideband MIMO antennas have been developed. In [5], a wideband microstrip MIMO antenna system with common elements for WiFi and LTE wireless access points was proposed. In [6], dual-polarized triple-band multibeam MIMO antennas were evaluated for WLAN/WiMAX access point applications. A MIMO antenna system for deployment in notebook computers for LTE/WWAN/WLAN applications was presented in [7]. In [8], a wideband 2×2 MIMO antenna with two bent slits and an operating band of 89% was introduced. Furthermore, a wideband 2×2 MIMO antenna for mobile applications with a 90% relative bandwidth was presented in [9].

Received 19 October 2018, Accepted 22 February 2019, Scheduled 21 March 2019

* Corresponding author: Alireza Moradi (alimoradi2020@gmail.com). ALIREZA MORADI is a researcher at Universiti Teknologi Malaysia under a Post-Doctoral Fellowship Scheme for the following Project: MIMO ANTENNA DESIGN FOR SIMULTANEOUS WIRELESS INFORMATION AND POWER TRANSFER (SWIPT) SYSTEM FOR 5G APPLICATIONS.

¹ Universiti Teknologi Malaysia, Malaysia. ² University of Surrey, UK.

WAP is a fundamental part of any wireless broadband access (WBA). WBA is a technology that provides computer networking access or high-speed wireless Internet access over a wide area. There are many reasons for utilizing the WAP in WBA. These include superior coverage, significant performance boost, reduced service turn-up costs, fixed demarcation points and reduced helpdesk costs [10]. However, WAP device performance is a function of antenna gain, directivity and orientation. For AP or router applications, monopole antennas are widely used, especially with high-gain and directional/omnidirectional radiation patterns [11]. Due to the demand for antennas for MIMO systems, several antenna designs have been proposed for use in AP devices, including a dual-loop antenna design suitable for a three-antenna system operating in the 2.4 and 5.2/5.8 GHz bands [12], a printed slot antenna with a cavity back and wideband operation bandwidth from 2.5 to 4.8 GHz [13], and a multiband printed meandered loop antenna with a coverage of the 4G LTE (699–798 MHz) band, UMTS (DCS/PCS) (1.7–2.0 GHz), WiMAX (2.3 and 3.5 GHz), and WLAN bands (2.4 and 5 GHz) [14]. However, to the authors' knowledge, all of the antennas reported in the aforementioned studies can only support up to 2×2 MIMO systems.

In this paper, a wideband MIMO antenna system (an improvement on previous work [15]) suitable for indoor or outdoor WAP and able support up to 4×4 MIMO systems while also providing diversity polarization with high gain is presented. The antenna system consists of four CPW-fed monopole antennas with a common ground plane and a radiated element with an operating frequency band of 2.25–2.75 GHz, which is appropriate for WiFi (2.4 GHz) and LTE (2.6 GHz, Malaysia) applications. To improve the mutual coupling between the proposed MIMO antenna ports, a parasitic element is introduced. The proposed antenna demonstrates satisfactory performance in terms of its reflection coefficients, coupling coefficients, diversity gain, and radiation characteristics. In Section 2, the geometry and fabrication process of the presented antenna are described in detail. The working mechanism of the parasitic element is studied in Section 3. In Section 4, simulated and measured results including surface current distribution, scattering parameters, radiation characteristics and received signal strength indicator are discussed. Finally, a conclusion is related in Section 5.

2. ANTENNA GEOMETRY AND FABRICATION

Recently, various combinations of different techniques for fabricating radiated element shapes and feeding structures for printed monopole antennas have been adopted by researchers to improve their impedance bandwidth. One type of widely used simple geometric technique is the staircase (stepped line) technique. With this technique, the corners of the radiated element of the printed monopole

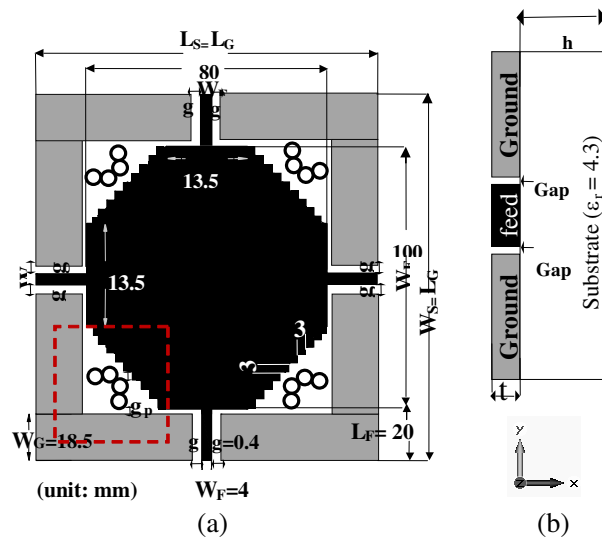


Figure 1. Geometry of the MIMO antenna system. (a) Top view. (b) Side view.

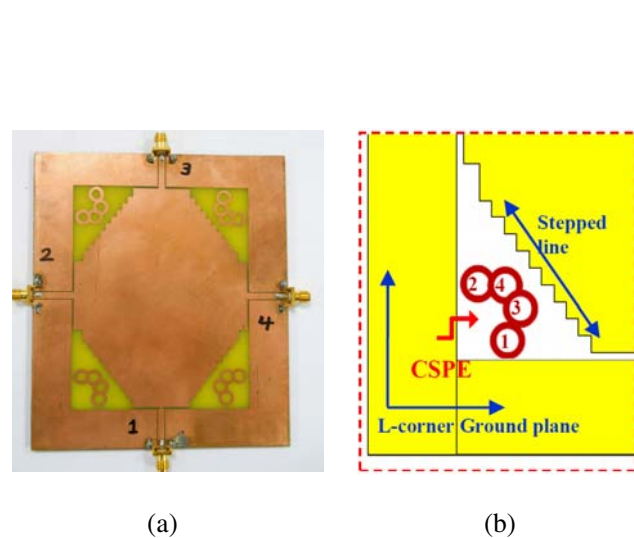


Figure 2. (a) Photograph of the fabricated prototype. (b) CSPE structure.

antenna are created with a stepped line profile to obtain the desired operating frequency band [16–19]. The design procedure for the proposed MIMO antenna system is based on this staircase technique.

Figure 1(a) shows the top view of the geometric details of the proposed MIMO antenna system, which consists of four CPW-feeds, a common radiator, and a ground plane. It can be seen that the gap (g) between the radiated element and the ground plane, as well as the width (W_F) and length (L_F), of the feed are identical for all ports. Fig. 1(b) shows the side view of the proposed MIMO antenna.

The fabricated prototype of the MIMO antenna system is pictured in Fig. 2(a). The MIMO antenna was designed and simulated using CST Microwave Studio software. The antenna is built on a FR-4 substrate with $\epsilon_r = 4.3$, $h = 1.6$ mm, loss tangent = 0.025, $W_S = 140$ mm and $L_S = 120$ mm. According to the CPW-fed structure, the radiated element and the ground plane, made of copper material ($t = 0.035$ mm, conductivity $\sigma = 5.96e7$ s/m), are etched on top of the substrate. The ground plane length and width are L_G and W_G , respectively.

3. PARASITIC ELEMENT STRUCTURE

Low isolation among the ports of a compact MIMO antenna system, in which components are tightly packed, is a big challenge. Low isolation degrades MIMO performance due to low antenna efficiency and high signal correlation. Several approaches have been used to increase isolation between the ports of a compact antenna, including the parasitic element (PE) technique [20], electromagnetic band-gap (EBG) structures [21], etching the meandered slot between the ports [22] and etching bent slits in the ground plane [23]. All of the aforementioned techniques decrease the reflection coefficient. Therefore, designing a wideband and high isolation antenna with common elements is very difficult.

As shown in Fig. 2(a), the structure of the design consists of four ports, all connected to the same radiated element and ground plane. Therefore, reducing the mutual coupling is one of the most critical tasks. Hence, a new PE structure, called the *chain shape parasitic element* (CSPE), is proposed to improve the mutual coupling between the four ports. Fig. 2(b) depicts the structure and position of the CSPE, which is illustrated in red. The dimensions of the rings are all as follows: $R_{in} = 5$ mm, $R_{out} = 7$ mm and $g_p = 1.5$ mm, where R_{in} is the inner radius of the rings, R_{out} is the outer radius of the rings, and g_p is the minimum gap between the rings and the ground plane or radiated element. One potential method to reduce current coupling and improve mutual coupling between the ports in this structure is changing the path of the current. Fig. 5 shows the current distribution of the presented antenna, in which the main current coupling among the ports flows via the L-corner ground plane and the stepped lines of the radiator. For this reason, the CSPE is located between the L-corner ground and the stepped line. After inserting the CSPE, a new coupling path is created, and a coupling current is accumulated. It should be noted that the rings of the CSPE help to trap the current coupling such

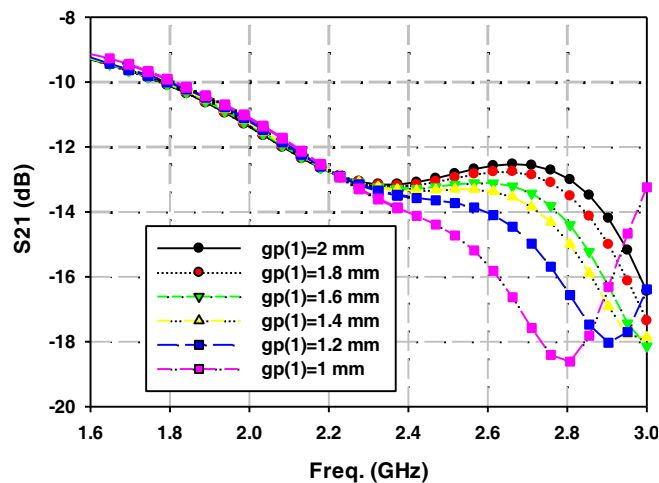


Figure 3. Parametric studies on the gap between the L-ground plane and ring number 1.

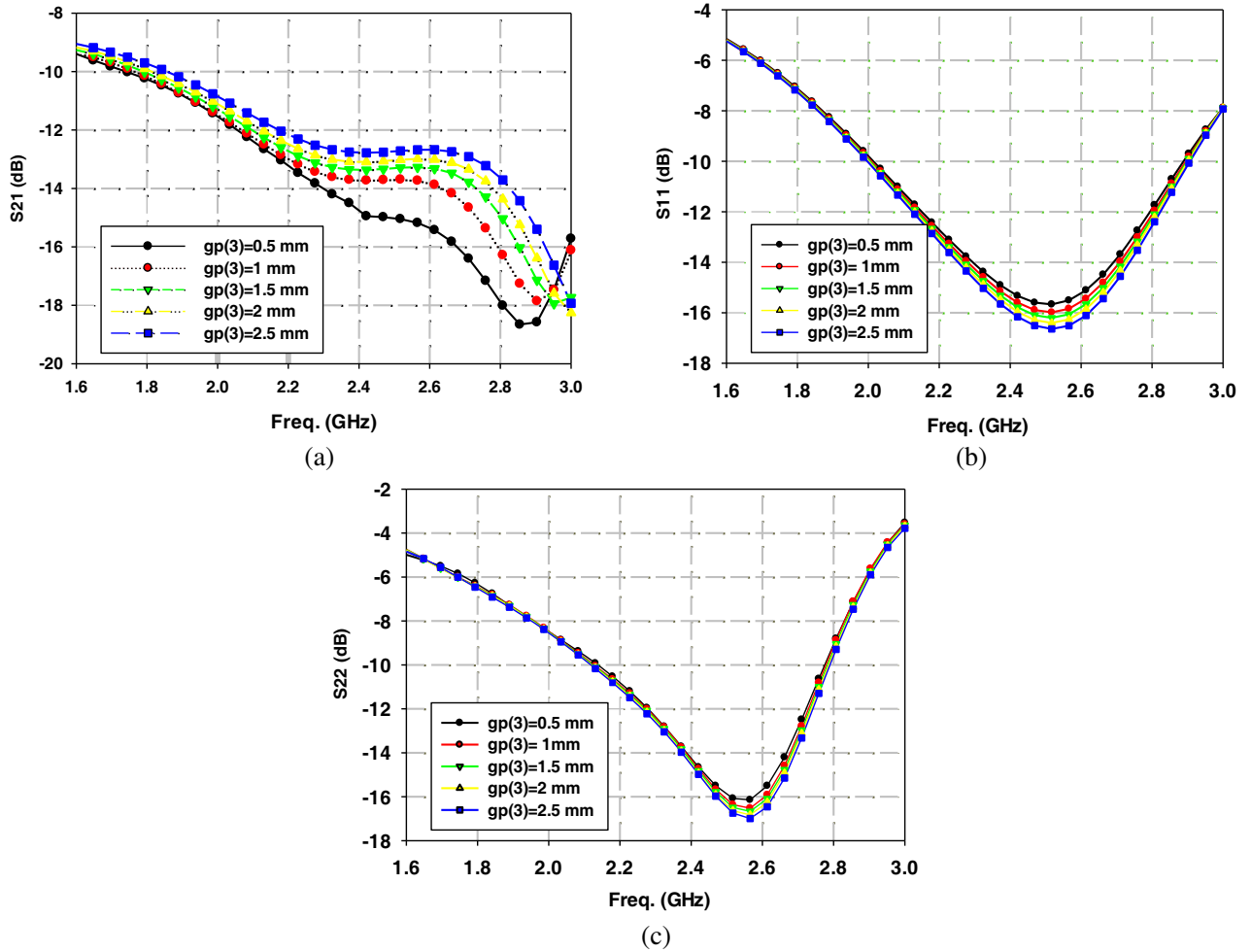


Figure 4. Parametric studies on the gap between the stepped line and ring number 3. (a) S_{12} . (b) S_{11} . (c) S_{22} .

that rings 1 and 2, via the L-ground plane, trap the current coupling, while the current coupling via the stepped line is accumulated through rings 3 and 4. Changing the location of the CSPE rings and moving them toward the ground plane and stepped line produces a number of results. The effect of varying the location of the CSPE rings on the coupling coefficient of the ports — in particular, a parametric examination of the effect of the gap between the L-ground plane and ring 1 — is illustrated in Fig. 3. It can be seen that as the gap is varied from 1 mm to 2 mm, S_{21} changes from -12.5 dB to -16 dB at a frequency of 2.6 GHz, for example. Additionally, Fig. 4 illustrates a similar examination of the stepped line and the gap between ring 3. As shown in Fig. 4(a), S_{21} varies from -12.5 dB to -15.5 dB at 2.6 GHz, at a range of gaps from 0.5 mm to 2.5 mm. Moreover, Figs. 4(b) and (c) indicate that S_{11} and S_{22} change approximately 1 dB at a range of gaps from 0.5 mm to 2.5 mm. The structure of the proposed antenna system is symmetric — thus, parametric studies of rings 2 and 4 are identical to those of rings 1 and 3, respectively.

4. SIMULATED AND MEASURED RESULTS

4.1. Surface Current Distribution

To study the effect of CSPE on the surface current of the presented MIMO antenna system, the current distributions of ports 1 and 2 at 2.6 GHz, with and without CSPE, are displayed in Fig. 5. For instance,

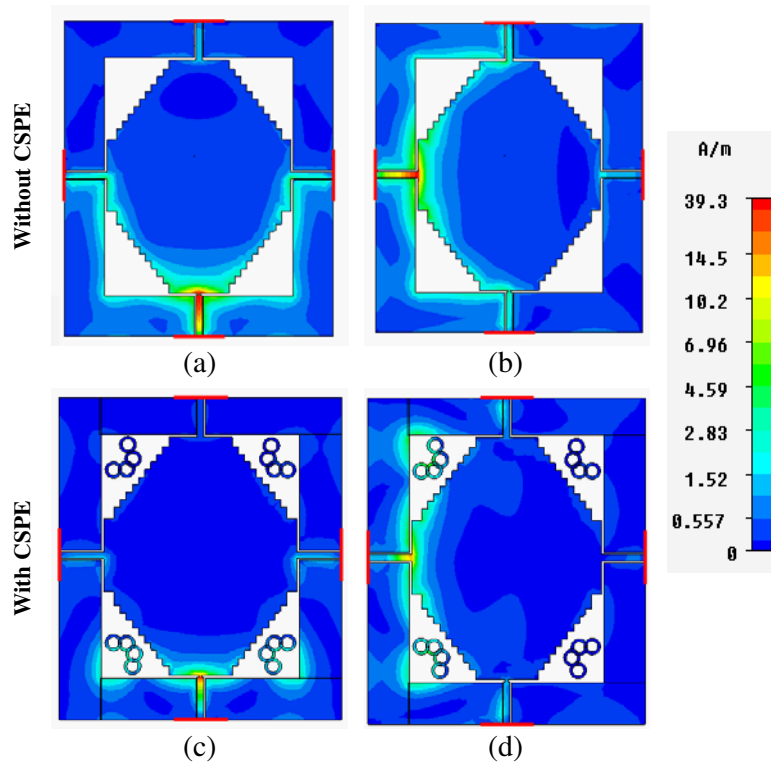


Figure 5. Current distributions of the MIMO antenna system with and without CSPE at 2.6 GHz. (a) Port 1 excited. (b) Port 2 excited. (c) Port 1 excited. (d) Port 2 excited.

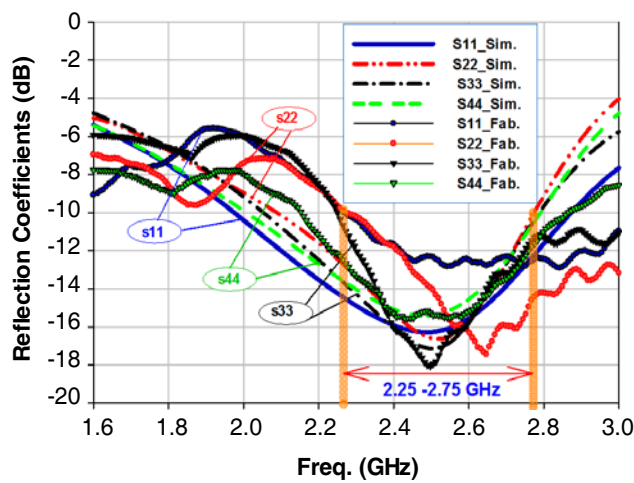


Figure 6. Comparison between the simulated and experimental measurements of reflection coefficients.

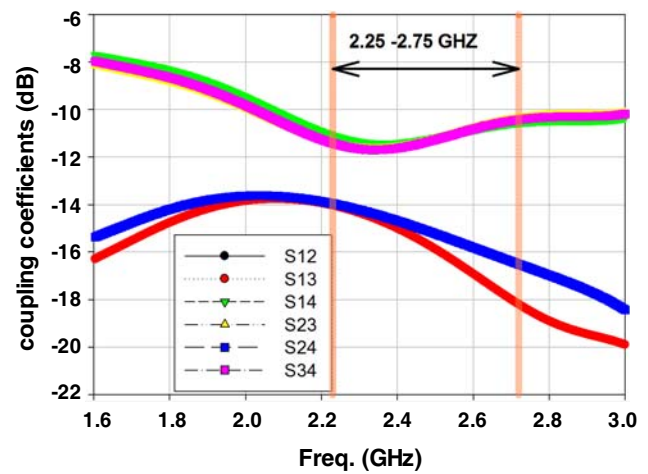


Figure 7. Simulated coupling coefficients of the MIMO antenna system without CSPE.

when port 1 is excited (Fig. 5(c)), a large portion of the surface current, which flows via the stepped line and the L-corner ground plane, is trapped at port 1 when CSPEs are used. Only a minimal coupling current is caught by the other ports. The other ports react similarly when they are excited. Therefore, when CSPEs are added, mutual coupling between the antenna ports is substantially reduced. As a result, the behavior of each port of the proposed antenna is the same as that of an independent antenna.

4.2. Scattering Parameters

To examine the validity of the simulation results and the scattering parameters obtained from the CST software, measurements were collected from a Rohde&Schwarz ZVL network analyzer. To obtain the measurements, three ports were terminated using three standard $50\ \Omega$ matching loads while the one remaining port was excited. Fig. 6 shows a comparison between the simulated and fabricated reflection coefficients for the presented MIMO antenna. The fractional bandwidth base at -10 dB was obtained at a frequency of 2.25–2.75 GHz, corresponding to approximately 20%. Therefore, the proposed antenna is suitable for WiFi (2.4 GHz) and LTE (2.6 GHz) applications. Comparisons between the simulated and measured results are divided into four groups of graphs, each with different colors; S_{11} , S_{22} , S_{33} and S_{44} are illustrated in blue, red, black, and green, respectively. The simulated and measured results seem to agree with one another.

Figure 7 shows the simulated coupling coefficients of the proposed MIMO antenna system without

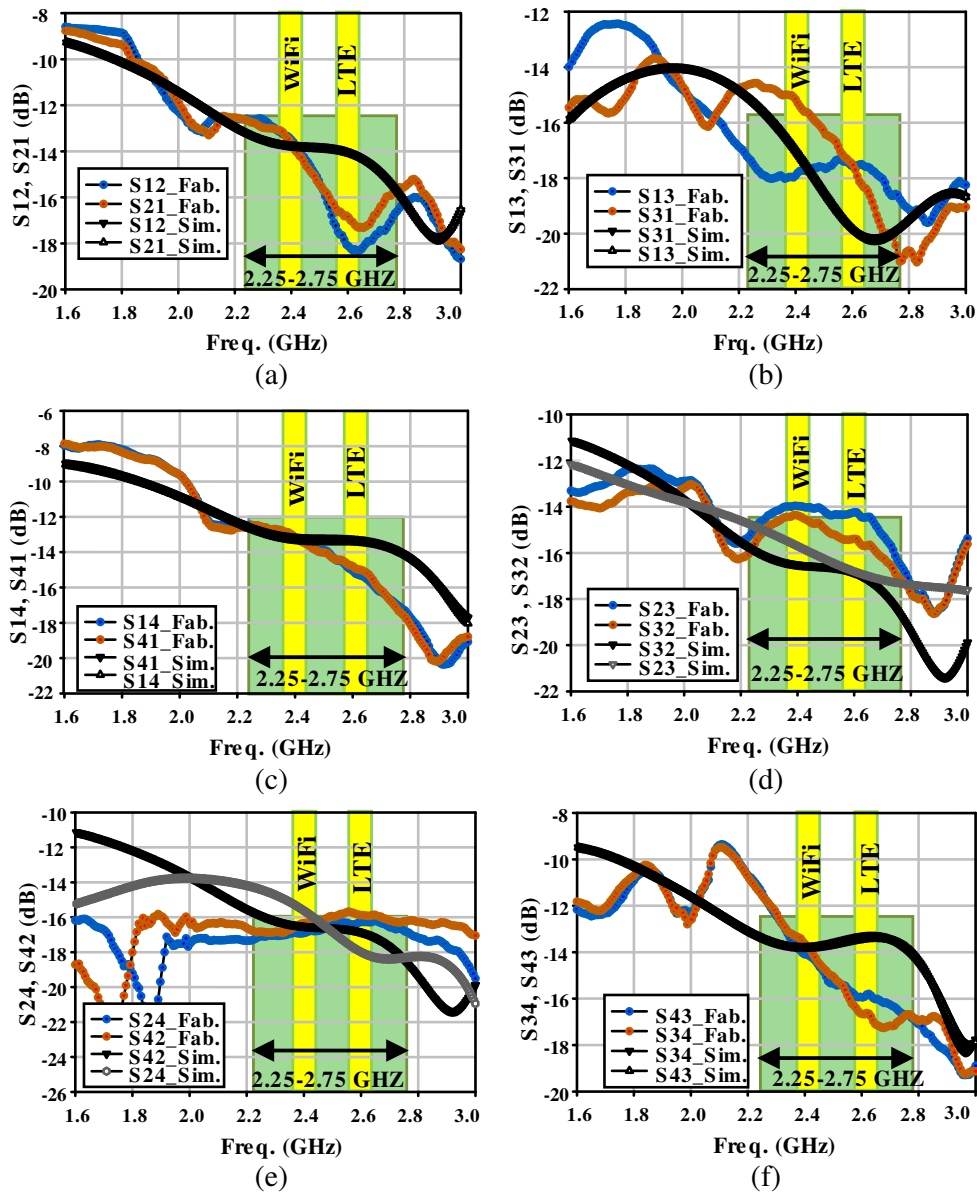


Figure 8. Simulated and measured coupling coefficients of the MIMO antenna system with CSPE. (a) S_{12} and S_{21} . (b) S_{13} and S_{31} . (c) S_{14} and S_{41} . (d) S_{23} and S_{32} . (e) S_{24} and S_{42} . (f) S_{34} and S_{43} .

CSPE. It can be seen that, except S_{24} and S_{13} , the results are approximately the same and all less than 12 dB.

Figure 8 represents the simulated and measured coupling coefficients of the MIMO antenna system, which are divided into six categories in the diagram. Each category corresponds to a comparison of the simulated and measured results between the two ports. Fig. 8(a) illustrates the values of S_{12} and S_{21} for ports 1 and 2. It may be observed that these values are higher than -14 dB in the WiFi and LTE frequency bands. The values of S_{13} and S_{31} for ports 1 and 3 are shown in Fig. 8(b). It can be seen that the values at the expected bandwidth (2.25–2.75 GHz) are below -15 dB. The values of S_{14} and S_{41} for ports 1 and 4 are shown in Fig. 8(c). The simulated results are quite similar to one another and approximately equal to -13 dB over the entire range of bandwidths, but the measured data are -13 dB and -15 dB at 2.4 and 2.6 GHz, respectively.

The diagrams in Fig. 8(d) illustrate the values of S_{23} and S_{32} for ports 2 and 3. It is apparent from the figure that the results at the desired bandwidth are below -14 dB. The measured value of S_{24} , which is shown in Fig. 8(e), is similar to that of S_{42} and is equal to -16 dB at the expected bandwidth, while the simulated results are slightly different such that at 2.4 GHz, $S_{24} = -15.5$ dB and $S_{42} = -16.5$ dB, and at 2.6 GHz $S_{24} = -18$ dB and $S_{42} = -17$ dB. The values of S_{34} and S_{43} for ports 3 and 4 are shown in Fig. 8(f). At 2.4 GHz, the simulated and measured results have the same value of -14 dB, whereas at 2.6 GHz, the simulated value is -13.5 dB while the measured results are approximately -16 dB. Consequently, the diagrams in Fig. 8 demonstrate acceptable isolation between the antenna ports of the proposed MIMO antenna system.

4.3. Radiation Characteristics

Radiation pattern measurement setup in an anechoic chamber is shown in Fig. 9.

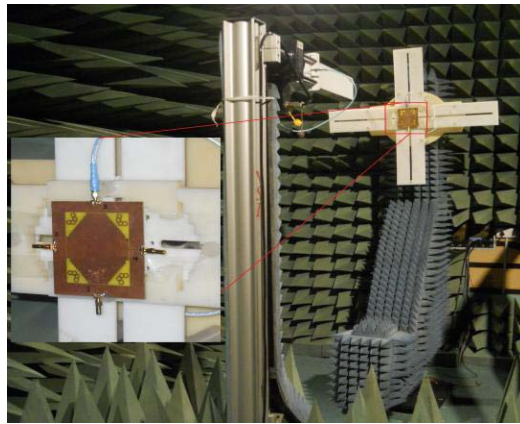


Figure 9. Measurement of radiation characteristics of the MIMO antenna.

A comparison of the normalized simulated and measured 2-D radiation patterns (E -plane and H -plane) of the MIMO antenna system at 2.4 and 2.6 GHz is shown in Fig. 10. The simulated data are generated using CST software and the measured data are collected in an anechoic chamber with one port excited and the other three ports terminated with a standard $50\ \Omega$ matching load. Because the results for ports 1 and 2 are identical to those for ports 3 and 4, respectively, only the radiation patterns for one pair of ports are shown. The structure of the ports is in the orthogonal mode; hence, a dual polarized MIMO antenna system is achieved. Therefore, the horizontal and vertical electric fields are produced from ports 1 and 2, respectively. Moreover, a nearly omnidirectional radiation pattern, without any deep nulls, is obtained at the expected operating frequencies.

To provide good diversity performance, the acceptable value of ECC should be less than 0.5 ([8] and [24]). Plots of the envelope correlation coefficient (ECC) between the ports of the presented MIMO antenna through the far-field are shown in Fig. 11. At the expected frequency band from 2.25 to 2.5 GHz,

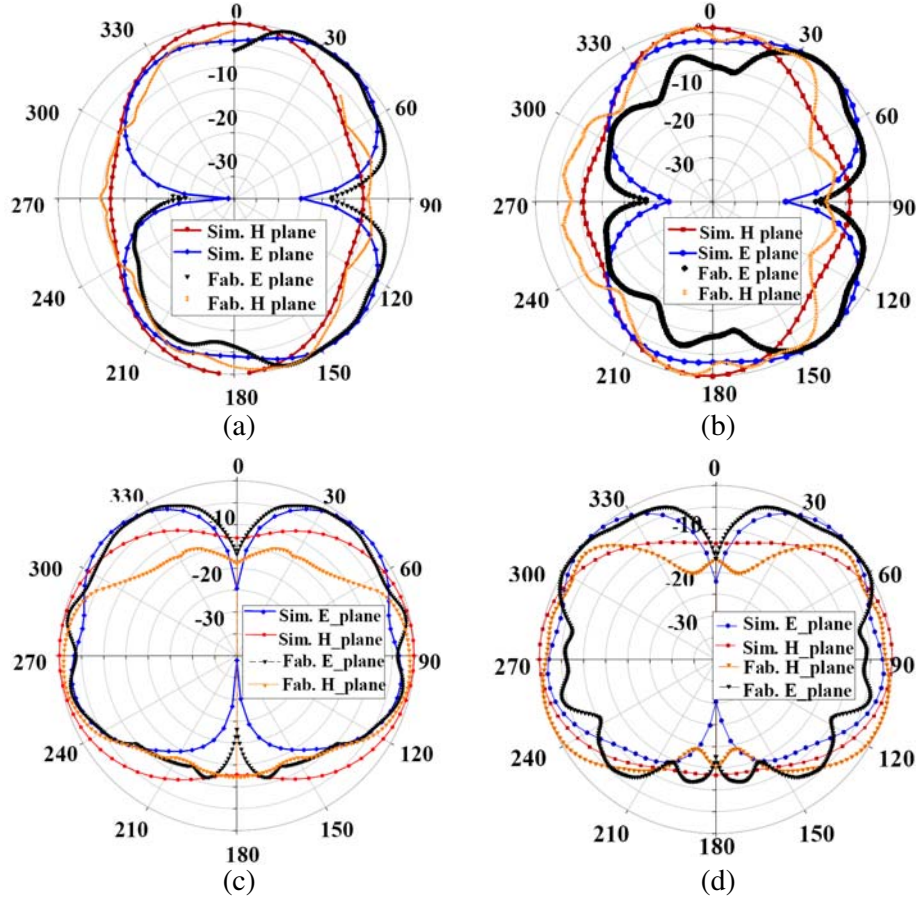


Figure 10. Normalized simulated and measured radiation pattern of the MIMO antenna system. (a) *E*-plane (y - z plane) and *H*-plane (x - z plane) of port 1 at 2.4 GHz. (b) *E*-plane (y - z plane) and *H*-plane (x - z plane) of port 1 at 2.6 GHz. (c) *E*-plane (x - z plane) and *H*-plane (y - z plane) of port 2 at 2.4 GHz. (d) *E*-plane (x - z plane) and *H*-plane (y - z plane) of port 2 at 2.6 GHz.

an ECC value of less than 0.2 is achieved, which is sufficient for MIMO applications. The ECC can be calculated by:

$$\rho = \frac{|S_{11}^* S_{12} + S_{12}^* S_{22} + S_{13}^* S_{32} + S_{14}^* S_{42}|^2}{\left(1 - (|S_{11}|^2 + |S_{21}|^2 + |S_{31}|^2 + |S_{41}|^2)\right) \left(1 - (|S_{13}|^2 + |S_{23}|^2 + |S_{33}|^2 + |S_{41}|^2)\right)} \quad (1)$$

Figure 12 shows plots of the simulated diversity gain for the MIMO antenna when the CSPE is located between the ports. It may be seen that, in the expected frequency bandwidth, gain values of approximately 10 dB are achieved.

Figures 13 and 14 show the simulated and measured peak gains and efficiencies of the proposed MIMO antenna for the four ports when one port is excited and the other ports are terminated. It may be observed that the coverage frequency of the simulated results is 1.6–3.0 GHz, which provides simulated peak gains of 3.5–7.6 dBi and efficiencies of 28–72%. The measured data, which were collected at the expected frequency bands of 2.4 and 2.6 GHz, produced peak gains of 5.0–6.97 dBi and measured efficiencies of 51.5–57%. Comparing the simulated and measured results demonstrates that they agree well with one another.

Table 1 compares the performance of the proposed design to other 4×4 MIMO antenna systems that appeared in literature.

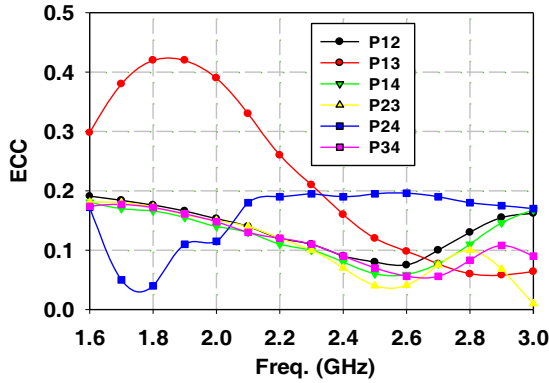


Figure 11. Far field envelope correlation coefficient.

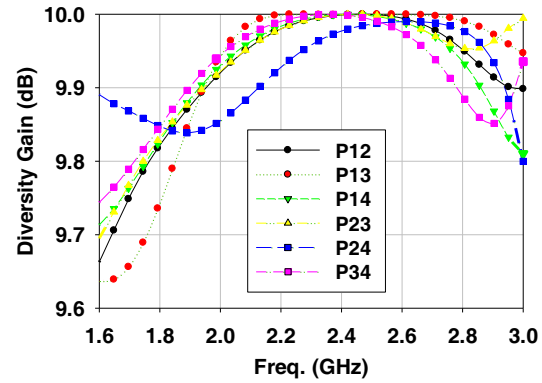


Figure 12. Simulated far-field diversity gain of the MIMO antenna system.

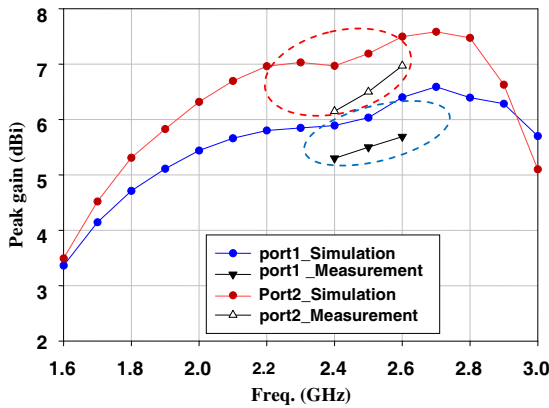


Figure 13. Simulated and measured realized gain of the MIMO antenna system with either port 1 or port 2 excited.

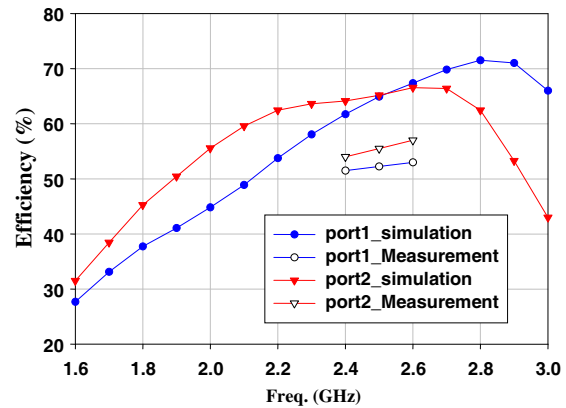


Figure 14. Simulated and measured efficiency of the MIMO antenna system with either port 1 or port 2 excited.

Table 1. A comparison table between the proposed MIMO antenna design and others.

Ref.	Frequency (GHz)	No. ports	Area mm ²	ECC (dB)	Peak Gain (dBi)	Efficiency (%)
[8]	2.4–6.55	2	40 × 78	0.01	0.22	46
[12]	2.4/5.8	3	120 × 120	< 0.3	7	80
[14]	2.3–2.5	4	150 × 150	< 0.5	3.2	58
[22]	2.4–2.84	2	101 × 60	< 0.41	3.46	81
This work	2.25–2.75	4	140 × 120	< 0.2	6.97	57

4.4. Received Signal Strength Indicator (RSSI) Measurement

The proposed antenna is designed for a WiFi/LTE router with two types of wireless cards, including a mini PCI WiFi card and a mini PCI LTE card. The mini PCI WiFi card can be used in either the 2.4 GHz or 5 GHz frequency bands. The mini PCI LTE card offers connectivity on 800/900/1800/2100/2600 MHz networks. Both wireless cards can support a 2 × 2 MIMO system. Based on the proposed MIMO antenna system structure, there are 6 scenarios for integrating the antenna with router-antenna cables. The WiFi/LTE antenna connections can integrate with ports 1/2, 1/3, 1/4, 2/3, 2/4 or 3/4. Based on the structure of the antenna, ports 1/3 and 2/4 possess identical polarization and a higher correlation

coefficient than the other 4 scenarios. Therefore, these two scenarios are not considered. However, the other 4 scenarios provide dual polarization, which is sufficient for 2×2 MIMO and even 4×4 MIMO applications. For example, the LTE and WiFi antenna cable connections can connect to ports 2/3 and 1/4, respectively, for a 2×2 MIMO system.

To ensure the signal distribution of the proposed antenna, a site survey was carried out using AirMagnet survey software. A site survey may be viewed as an in-depth examination and analysis of a proposed WiFi/LTE site. The primary objective of the survey tool is to ensure that the mobile client station receives good signals and a high transmission throughput rate in the area where it operates. It also determines the number of access points and the placement of those access points. The AirMagnet survey software was used to show the coverage and strength of the signal from ports 1 and 2 of the proposed MIMO antenna system. The measured data were collected by AirMagnet version 6 with a wireless PC Card able to support 802.11a/b/g/n for real-time analysis. The received signal strength index (RSSI) measurement of the WiFi site in a building of size $40 \times 40 \text{ m}^2$ was also determined. The building's main walls were composed of concrete, while the interior walls were brick. Due to the limitations of wireless networks, the RSSI measurement was carried out for only a single-input single-output (SISO) WiFi system. Fig. 15(a) shows the WAP with the proposed antenna under test, which was mounted on a ceiling. The WAP was located inside and approximately at the center of the building at a fixed position. The proposed antenna was connected, via the WiFi cable connections, to the WiFi/LTE router (Fig. 15(b)). The architecture of the router, including mini PCI wireless cards and antenna cable connections, is illustrated in Fig. 15(c). A laptop able to support the AirMagnet 802.11 wireless PC card and able to measure and analyze the RSSI was used as a receiver. It is shown in Fig. 15(d).

As shown in Figs. 16 and 17, the RSSI measurement, obtained using AirMagnet software, is measured in dBm. Different colors are used to identify various RSSI levels in the system coverage range on ports 1 and 2, respectively. The areas identified in light blue and green possess the best signal quality, with RSSI between -25 to -65 dBm, while the areas in yellow possess weaker signal strengths

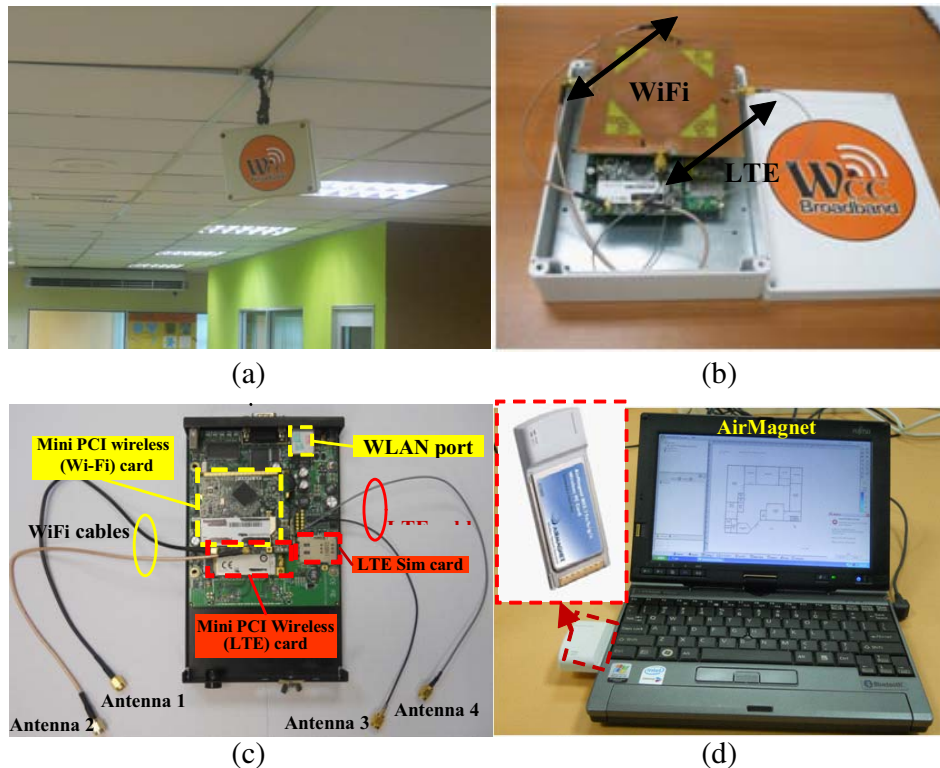


Figure 15. (a) Ceiling-mounted WAP. (b) The proposed antenna integrated with the WAP. (c) Architecture of a WiFi/LTE router. (d) Receiver laptop (with AirMagnet wireless PC Card).

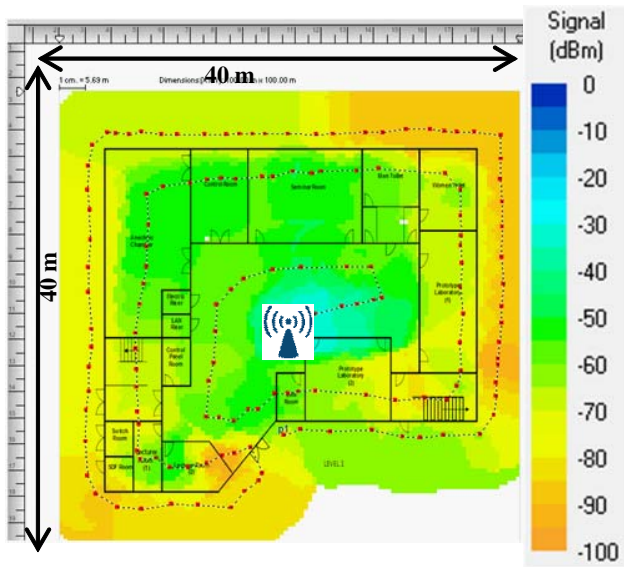


Figure 16. RSSI measurement for port 1.

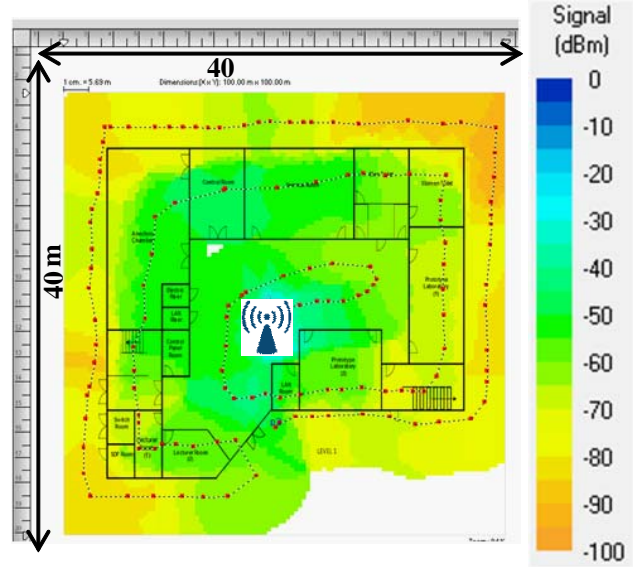


Figure 17. RSSI measurement for port 2.

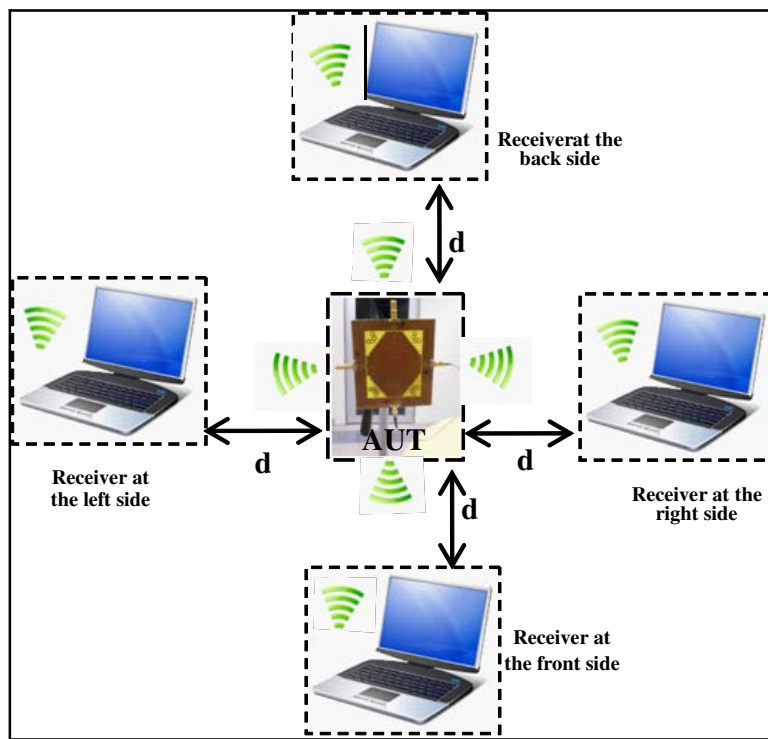


Figure 18. Measurement of RSSI at four points around the AUT.

between -65 to -80 dBm. The areas with the weakest signal quality, with RSSI less than -80 dBm, are indicated in brown. In these areas, the possibility of the signal being cut off is high. The dotted lines on the maps signify the receiver path (laptop) taken during the measurement process, while the red points denote measurement points.

To ensure a nearly omnidirectional pattern for the proposed antenna when integrated with a WAP, an RSSI measurement value processed in four different directions was considered. For this measurement, the WAP was located at the fixed point with four receivers (laptops) placed around

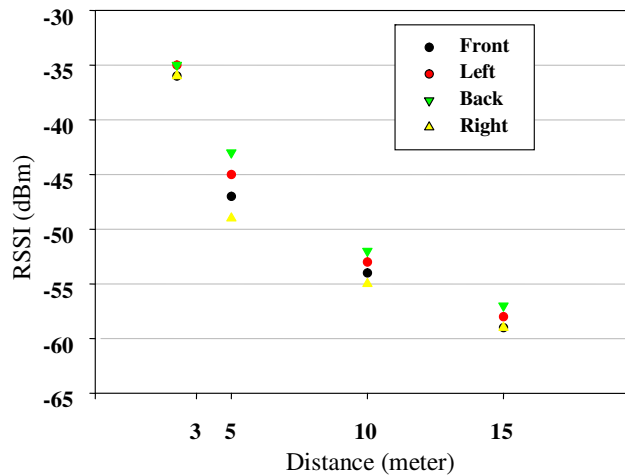


Figure 19. Measured RSSI of port 1 on four sides of the AUT at different distances.

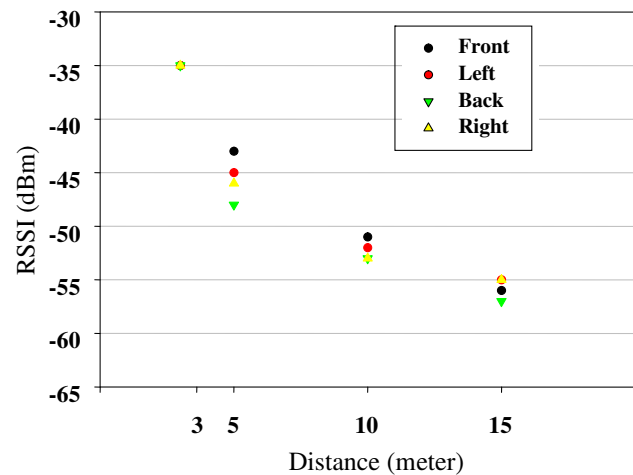


Figure 20. Measured RSSI of port 1 on four sides of the AUT at different distances.

it in four different directions, equidistant and without barrier between them. This setup configuration for RSSI measurement is shown in Fig. 18. The RSSI measurement for 2.4 GHz was performed for port 1 and port 2 at distances of 3, 5, 10 and 15 meters from the antenna under test (AUT). As previously mentioned, the RSSI measurements were obtained using the AirMagnet software, with the wireless data collected from AirMagnet 802.11 wireless PC card for real-time analysis. The measured RSSI results for ports 1 and 2 without barrier are shown in Figs. 19 and 20, respectively. It may be seen that there is good agreement between measured data at the same distances, which confirms the omnidirectionality of the proposed antenna.

5. CONCLUSION

A new wideband MIMO antenna system suitable for indoor or outdoor wireless access point applications, made up of four CPW-fed monopole antennas, is presented. The simulated and measured results show that the four antennas (ports 1–4) provide frequency bands from 2.25 GHz to 2.75 GHz, based on their reflection coefficients, which are below -10 dB. Due to the common element structure, a chain shape parasitic element is introduced to improve the mutual coupling between the ports so that coupling coefficients better than -14 dB are achieved. A calculated envelope correlation coefficient, with regard to the far field, is obtained to evaluate the diversity performance of the proposed antenna; this coefficient is less than 0.2. The covered frequency band, according to the S -parameters and radiation characteristics, makes it a good candidate for WiFi and LTE MIMO applications.

ACKNOWLEDGMENT

The authors would like to acknowledge and express sincere appreciation to Research Management Centre (RMC) of Universiti Teknologi Malaysia for financing this project.

REFERENCES

1. Ban, Y.-L., et al., "4G/5G multiple antennas for future multi-mode smartphone application," *IEEE Access*, Vol. 4, 2981–2988, 2016.
2. Wang, C.-J. and C.-M. Lin, "A CPW-fed open-slot antenna for multiple wireless communication systems," *IEEE Antennas Wireless Propag. Lett.*, Vol. 11, 620–623, 2012.
3. Liu, W.-C., "Broadband dual frequency meandered CPW-fed monopole antenna," *Electron Lett.*, Vol. 40, 1319–1320, 2004.

4. Lu, W.-C., "Broadband dual frequency cross-shaped slot CPW-fed monopole antenna for WLAN operation," *Microwave Opt. Tech. Lett.*, Vol. 46, 353–355, 2005.
5. Moradi Kordalivand, A., T.-A. Rahman, and M. Khalily, "Common elements wideband MIMO antenna system for WiFi/LTE access-point applications," *IEEE Antennas Wireless Propag. Lett.*, Vol. 13, 1601–1604, 2014.
6. Pan, Y., et al., "Evaluation of dual-polarised triple-band multibeam MIMO antennas for WLAN/WiMAX application," *IET Microwaves, Antennas & Propagation*, Vol. 11, 1469–1475, 2017.
7. Chen, S.-C. and C.-S. Fu, "Switchable long-term evolution/ wireless wide area network/ wireless local area network multiple-input and multiple-output antenna system for laptop computer," *IEEE Access*, Vol. 5, 9857–9865, 2017.
8. Li, J.-F., Q.-X. Chu, and T.-G. Huang, "A compact wideband MIMO antenna with two novel bent slits" *IEEE Trans. Antennas Propag.*, Vol. 60, No. 2, 482–489, Feb. 2012.
9. Sonkki, M., E. Antonino-Daviu, M. Cabedo-Fabrés, M. Ferrando-Bataller, and E. T. Salonen, "Improved planar wideband antenna element and its usage in a mobile MIMO system," *IEEE Antennas Wireless Propag. Lett.*, Vol. 11, 826–829, 2012.
10. WiMAX: *Broadband Wireless Access*, Wi-fiplanet.com, retrieved Mar. 2008.
11. Li, R. L., X. L. Quan, Y. H. Cui, and M. M. Tentzeri, "Directional triple-band planar antenna for WLAN/WiMax access points," *Electron Lett.*, Vol. 48, No. 6, 2012.
12. Su, S.-W., "High-gain dual-loop antennas for MIMO access points in the 2.4/5.2/5.8 GHz bands," *IEEE Antennas Wireless Propag. Lett.*, Vol. 58, No. 7, 2412–2419, 2010.
13. Medeiros, C. R., E. B. Lima, J. R. Costa, and C. A. Fernandes, "Wideband slot antenna for WLAN access points," *IEEE Antennas Wireless Propag. Lett.*, Vol. 9, 79–82, 2010.
14. Fernandez, S. C. and S. K. Sharma, "Multiband printed meandered loop antennas with MIMO implementations for wireless routers," *IEEE Antennas Wireless Propag. Lett.*, Vol. 12, 96–99, 2013.
15. Moradi, A., T.-A. Rahman, C. Y. Leow, and S. Ebrahimi, "Dual-polarized MIMO antenna system for WiFi and LTE wireless access point application," *Int. J. Commun. Syst.*, Vol. 30, 2017.
16. Kim, S. J., H. S. Lee, and Y.-S. Kim, "A CPW-fed staircase monopole UWB antenna with band-notched frequency in the WLAN band," *Microw. Opt. Technol. Lett.*, Vol. 49, No. 10, 2545–2547, 2007.
17. Azarmanesh, M., S. Soltani, and P. Lotfi, "Design of an ultra-wideband monopole antenna with WiMAX, C and wireless local area network band notches," *IET Microw. Antennas Propag.*, Vol. 5, No. 6, 728–733, 2011.
18. Zaker, R. and A. Abdipour, "A very compact ultrawideband printed omnidirectional monopole antenna," *IEEE Antennas Wireless Propag. Lett.*, Vol. 9, 471–473, 2010.
19. Kim, K.-H., Y.-J. Cho, S.-H. Hwang, and S.-O. Park, "Band-notched UWB planar monopole antenna with two parasitic patches," *Electron Lett.*, Vol. 41, No. 14, 2005.
20. Zhou, X., X.-L. Quan, and R.-L. Li, "Dual-band WLAN diversity antenna system with high port-to-port isolation," *IEEE Antennas Wireless Propag. Lett.*, Vol. 11, 244–247, 2012.
21. Yang, F. and Y. Rahmat-Samii, "Microstrip antennas integrated with EBG structures: A low mutual coupling design for array applications," *IEEE Trans. Antennas Propag.*, Vol. 51, 2936–2946, Oct. 2003.
22. Ayatollahi, M., Q. Rao, and D. Wang, "A compact, high isolation and wide bandwidth antenna array for long term evolution wireless devices," *IEEE Trans. Antennas Propag.*, Vol. 60, No. 10, 4960–4963, Oct. 2012.
23. Li, J.-F., Q.-X. Chu, Z.-H. Li, and X.-X. Xia, "Compact dual band-notched UWB MIMO antenna with high isolation," *IEEE Trans. Antennas Propag.*, Vol. 61, No. 9, 4759–4766, Sep. 2013.
24. Colburn, J. S., Y. Rahmat-Samii, M. A. Jensen, and G. J. Pottie, "Evaluation of personal communications dual-antenna handset diversity performance," *IEEE Trans. Antennas Propag.*, Vol. 47, No. 3, 737–746, Aug. 1998.